Engineering Solid Mechanics 10 (2022) 373-386

Contents lists available at GrowingScience

Engineering Solid Mechanics

homepage: www.GrowingScience.com/esm

The behavior of self compacting concrete exterior beam-column joints with a variation of shear reinforcement against cyclic lateral loads

Saloma[a], Siti Aisyah Nurjannah[a*], Arie Putra Usman[a], Yakni Idris[a], Ika Juliantina[a] and Rieske Calista Viegra Effendy[a]

[a]*Civil Engineering Department, Faculty of Engineering, Universitas Sriwijaya, Indralaya 30662, Indonesia*

ARTICLE INFO

Article history:
Received 27 January 2022
Accepted 27 May 2022
Available online
27 May 2022

Keywords:
Cyclic lateral loads
Ductility
Exterior Beam-Column Joints
Finite Element Method
Self Compacting Concrete

ABSTRACT

The beam-column joints are designed to have sufficient capacity under earthquake loads. This requirement needs design details of reinforcement that fulfill the seismic criteria and adequate compaction of concrete. Using Self Compacting Concrete (SCC) material can solve the difficulty of compacting conventional concrete due to the close reinforcement distance. This study aimed to analyze the behavior of the Exterior Beam-column Joints (EBJ) using SCC as materials with a variation of shear reinforcements to withstand cyclic lateral loads. The analysis was carried out using the ANSYS software and the Finite Element Method. The analysis included hysteresis curves, stress contours, ductility, stiffness, and structural strength. The performance of an EBJ without shear reinforcement (EBJ-S1 model) was compared to other EBJs using horizontal (EBJ-S2 model) and diagonal (EBJ-S3 model) shear reinforcements in the joint zones. The results showed that horizontal and diagonal shear reinforcement in the joint zones affected the performance of the EBJs in resisting cyclic lateral loads as the representative of earthquake loads. The EBJ without shear reinforcement could withstand compressive stresses of 3.33 to 17.22 MPa, while both EBJs using horizontal and diagonal shear reinforcement achieved the same compressive stresses range of 3.33 to 20 MPa. The EBJ with diagonal reinforcement performed a wider compressive area of stress contour than the EBJ of horizontal reinforcement. The EBJ-S3 model achieved the highest ductility value of 4.733 with diagonal shear reinforcements because it achieved the highest ultimate displacement of the other EBJ models.

1. Introduction

The quality of the beam-column joints determines post-earthquake structural failure. The appropriate design is needed to provide strength and ductility and prevent collapse due to shear forces. This incident can be solved by adding shear reinforcement according to the seismic code criteria. Shear reinforcement can be designed in several ways. In some designs, the close distances of shear reinforcement in the joint zones cause the pouring and compacting of conventional concrete increasingly difficult. Compaction aims to minimize air voids trapped in the concrete during the casting. If the concrete compaction is not perfect, it reduces deformation and causes vulnerability of joints due to earthquakes.

Concrete materials with easy flow properties are needed to ensure concrete compaction, especially in the joint zones. One material that has these properties is Self Compacting Concrete (SCC). The casting of SCC does not require vibrators because SCC can flow and compact due to its weight (Brouwers and Radix, 2005). The nature of SCC, which is very runny and more homogeneous, makes it able to fill the gaps between close distance steel reinforcements and formwork corners that the vibrators cannot reach. This behavior can avoid aggregate segregation (Islam, 2022). Moreover, SCC can be placed and compacted without a vibrator (Concrete, 2005; Jayaseelan et al., 2019).

* Corresponding author.
E-mail addresses: sitiaisyahn@ft.unsri.ac.id (S. A. Nurjannah)

doi: 10.5267/j.esm.2022.6.001

Some advantages of SCC materials include reducing aggregate use by up to 50%, reducing cement, and the association with CO2 production (Hanafiah, et. al., 2017; Islam, et al., 2022) are safer for the environment. One of the substitutes for aggregate is expanded clay to maintain the strength of SCC (Verzegnassi, et al., 2022). Although it has flow properties, SCC can be made without superplasticizers; then the manufacturing costs are reduced. Without using a superplasticizer in the mixture, SCC can achieve compressive strengths of 30 MPa to 37 MPa (Karthik et al., 2022) or 41.813 MPa to 67.239 MPa (Hanafiah et al., 2017).

The experimental works in the laboratories and numerical model using software are widely used to obtain Exterior Beam-column Joints (EBJ) performance under cyclic lateral loads. In the modeling process, a structural object is divided into smaller discrete elements that are connected by nodes to represent complex geometric shapes (Jagota et al., 2013; Ghouilem, et al., 2021). This study contains a comparison of the behavior of one EBJ model using NC and three EBJ models using SCC material that was carried out by numerical analysis. There were three variations of shear reinforcement in the joints of EBJs that perform to resist cyclic lateral loads. The analysis results were compared in the form of hysteresis curves, stress contours, ductility, strength, and stiffness. The load distribution in the reinforced concrete structures flows from beams to columns through beam-column connections, namely joints. The joints are subjected to compressive, tensile, and shear forces. The bearing capacity of the joints depends on the combined mechanism of longitudinal and transversal reinforcements. The joints must be designed to provide adequate bearing capacity in resisting seismic loads and inelastic deformation without reducing the strength of the structure. Joints are generally divided into three types, namely interior, exterior, and corner. The brittle behavior of concrete makes it unable to prevent shear cracks due to lateral cyclic loads, and then shear reinforcements are needed to be installed in the joints. The shear reinforcements in the joints are designed to withstand shear forces that exceed the shear strength of concrete and are generally arranged in horizontal, diagonal, and spiral shear reinforcements.

Ductility is defined as the ability in inelastic conditions without reducing the structural capacity to withstand loads. Based on a code (FEMA, 2000), ductility is classified into three types: low, medium, and high, with values of less than 2, ranging from 2 to 4, and higher than 4. In this study, the numerical analysis was conducted using ANSYS software for modeling the EBJs. The parts of EBJs resembled SOLID65, SOLID45, and LINK180 elements as representatives of the concrete, steel plate, and steel reinforcement, respectively. These elements discretized complex continuum domains interconnected through nodes (Pinto, at al., 2021). The stages in the problem-solving in the software are (Thompson & Thompson, 2017; ANSYS, 2013):

1. Preprocessing is defining the model by entering the geometric data, element types, and material properties.
2. The running program is the loading subjected to the structural models. The type of load applied follows the input and can be in constant monotonic load, increasing monotonic load, and cyclic load. At this stage, the analysis process is run by the software.
3. Postprocessing displays the analysis results in stress contours, deformation contours, crack locations, and data tables for strain, stress, force, and deformation.

2. Materials and method

2.1 Exterior Beam-Column Joint

This study used geometric data to model EBJs, the material properties of Normal Concrete (NC) and steel reinforcement, and the loading history based on previous research (Saghafi and Shariatmadar, 2018). The details of dimension and reinforcement are as described in Fig. 1 (redrawn). The Exterior Beam-Column Joint using NC (EBJ-NC) and using SCC (EBJ-S1) without shear reinforcement in the joint were not designed based on seismic criteria, while the EBJ-S2 in Fig. 2 (redrawn) fulfills the seismic requirement based on the code (ACI 318, 2011). In this study, a model of EBJ-S3 in Fig. 3 with diagonal shear reinforcements was also investigated. The cross-sectional dimensions of the column are (250×250) mm with 9ϕ14 longitudinal reinforcement and 10-60 stirrups. The cross-sectional dimensions of the beam are (220×250) mm with 4ϕ14 top, 3ϕ14 bottom longitudinal reinforcement, and 10-60 stirrups, with yield and ultimate strengths, which are written in Table 1. The beam-column joints were modeled with various shear reinforcements, as shown in Table 2. The compressive strength of NC was 32 MPa with an elastic modulus of 26587 MPa. The yield strengths of longitudinal reinforcing steels (ϕ14 and ϕ10) were 430 MPa and 387 MPa, respectively. The data properties of SCC were obtained from previous research by Hanafiah, et al. (2017) with an elastic modulus of 30391 MPa and 41.813 MPa of compressive strength.

Table 1. The properties of steel reinforcement (Saghafi and Shariatmadar, 2018)

Diameter	Yield Strength (MPa)	Ultimate Strength (MPa)
ϕ10	380	440
ϕ14	430	673

Table 2. Variation of shear reinforcements of Exterior Beam-Column Joints

Model	Concrete Material	Variation of Shear Reinforcement	Shear Reinforcement (Stirrup) in the Joints
EBJ-NC	NC	-	-
EBJ-S1	SCC	-	-
EBJ-S2	SCC	Horizontal	Ø10-60
EBJ-S3	SCC	Diagonal	Ø10; *l*=180mm

Notes: NC: Normal Concrete, SCC: Self Compacting Concrete; l: length

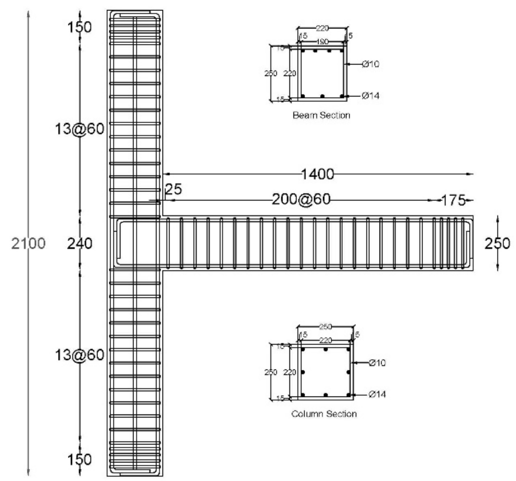

Fig. 1. EBJ-N1 and EBJ-S1 without shear reinforcement in the joint (Saghafi & Shariatmadar, 2018, redrawn)

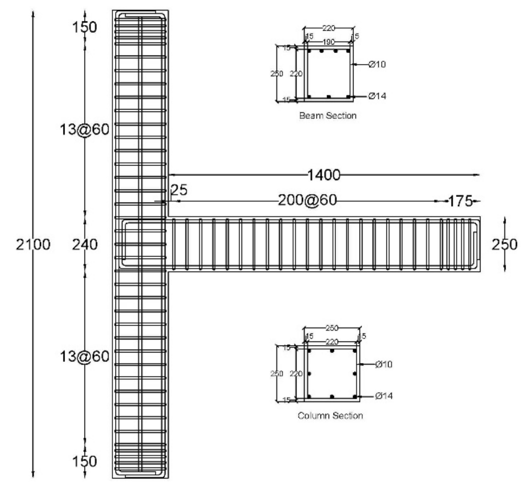

Fig. 2. EBJ-S2 with horizontal shear reinforcement (Saghafi & Shariatmadar, 2018, redrawn)

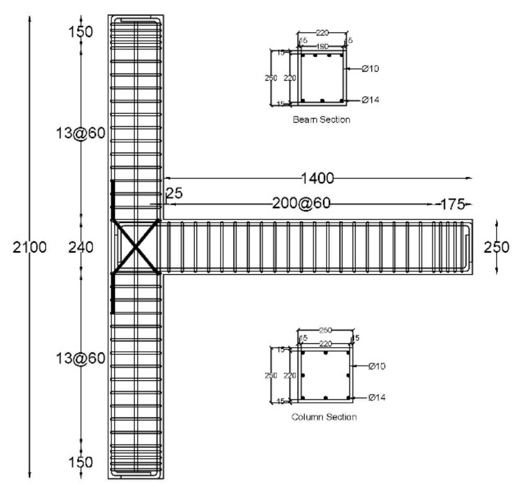

Fig. 3. EBJ-S3 with diagonal shear reinforcement

2.2 Elements in the Modeling of Exterior Beam-Column Joints

The ANSYS 2020 R1 software was used for EBJ modeling. The concrete, steel plates, and steel reinforcements were modeled as discrete elements of SOLID65, SOLID45, and LINK180, respectively. SOLID65 is a three-dimensional element with 8 nodes (8-node brick element) shown in Fig. 4. Each nodal is allowable to translate in the X, Y, and Z axes. SOLID65 elements can be modeled as elements that experience cracking due to tensile stress, crushing due to compression, and inelastic translation. A SOLID45 element is shown in Fig. 5 to represent a steel plate. It can be deformed to act as an intermediary between loading cells and an EBJ. The model of longitudinal and transverse reinforcing steel elements inside the EBJs used LINK180 elements. The axial force at the ends of the LINK180 rods is shown in Fig. 6. In this model, elements are formed through two nodes at the ends of the rods in the Cartesian coordinate. Each node is available to translate in the direction of three directions of axes. The element is not subject to bending, and stresses are assumed to be the same throughout the member. The application of the SOLID65 and SOLID45 elements on an EBJ model is presented in Fig. 7. Figs (8-10) show the LINK180 element application on EBJ-S1, EBJ-S2, and EBJ-S3 models.

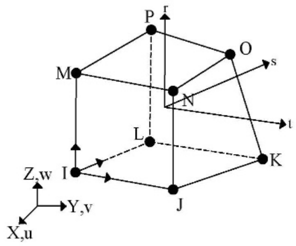

Fig. 4. SOLID65 element

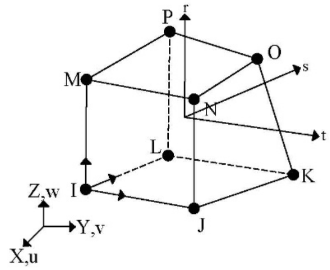

Fig. 5. SOLID45 element

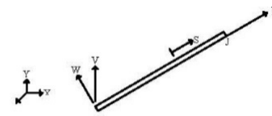

Fig. 6. LINK180 element

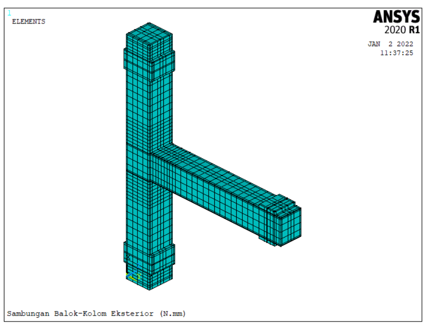

Fig. 7. SOLID65 and SOLID45 element modeling

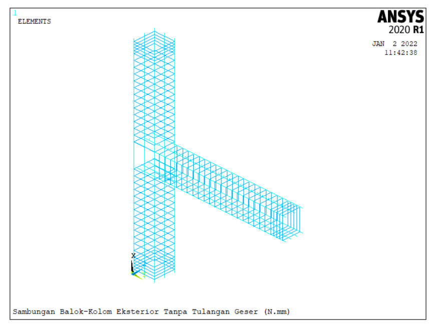

Fig. 8. LINK180 element modeling of EBJ-NC and EBJ-S1

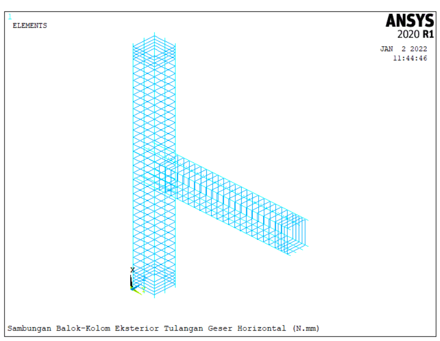

Fig. 9. LINK180 element modeling of EBJ-S2

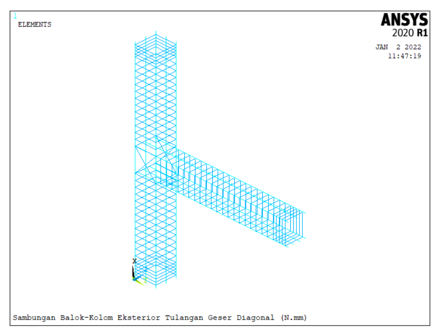

Fig. 10. LINK180 element modeling of EBJ-S3

2.3 Nonlinear Equations to Solve Numerical Solutions

There are some equations for solving the nonlinear equation in describing the behavior of EBJ models. One of them is the equation that describes a correlation between strain and displacement in Eq. (1) (Cook, 2007).

$$\{\varepsilon\} = [C]\{u\} \tag{1}$$

where,

$[C]$: matrix of strain displacement
$\{u\}$: vector of displacement

The correlation between the stiffness matrix [K] and [C] is described in Eq. (2). Eq. (3) expresses stiffness, deformation, and load matrices. The equation of a linear correlation is explained in Eq. (4).

$$[K] = [C]^T[D][C]\{u\}dV \tag{2}$$
$$[K]\{u\} = \{p\} \tag{3}$$
$$[K]\{u\} = \{F^b\} \tag{4}$$

where $[K]$, $\{u\}$ and $\{F^b\}$ are matrix of the stiffness, vector of dof and vector of load, respectively. In the nonlinear case, the Newton-Raphson iteration process is used to solve Eqs. (5) and (6) (Budiono, et. al., 2019). These equations represent an iteration to complete each addition of the displacement.

$$[K_f^T]\{\Delta u_f\} = \{F^b\} - \{F_f^{jq}\} \tag{5}$$

$$\{u_{f+1}\} = \{u_f\} + \{\Delta u_f\} \tag{6}$$

where $[K_i^T]$, $\{u_f\}$ and $\{F_f^{jq}\}$ are matrix of the stiffness, vector of dof and vector of load, respectively. The solution is obtained through several iterations using these steps:

1.Define a value of $\{u_o\}$ where $\{u_o\}$ is obtained from the previous iteration.
2.Define a matrix of $[K_i^T]$, $\{F_f^{jq}\}$ from $\{u_f\}$.
3.Define the matrix of $\{\Delta u_f\}$.
4.The matrix $\{\Delta u_f\}$ is added to $\{u_f\}$ to determine $\{u_{f+1}\}$.

Fig. 11 shows the solution for the next iteration. Some iterations involve a curve of load and displacement, resulting the load factor $\{F_i^{jq}\}$ is equal to $\{F\}$, or close to a specific tolerance value.

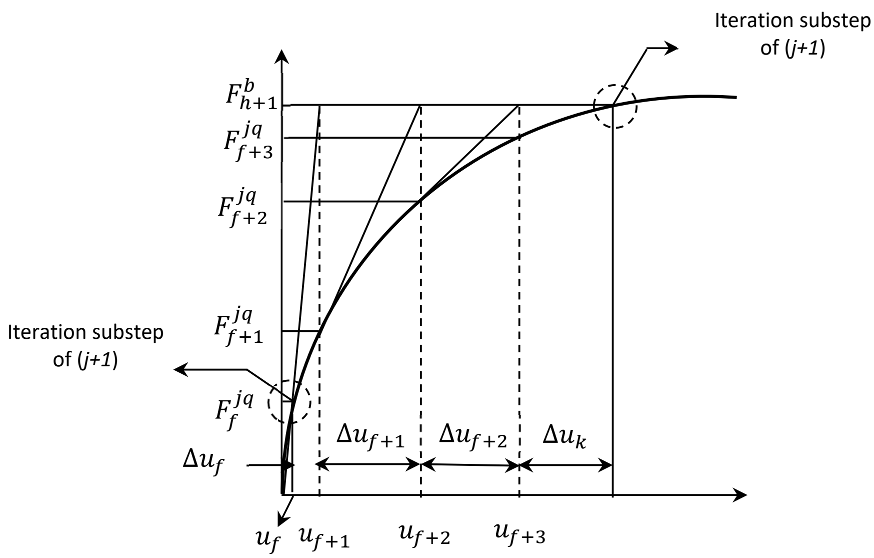

Fig. 11. Iteration of load factor based on Newton-Raphson method

The finite element method is compatible with solving cases of nonlinear equations that include large deformation on structures using iteration by applying the Newton-Raphson method. This method can solve problems in nonlinear algebraic equations using the evaluation in each iteration. The solution is assumed to be in the zone of attraction, and thus there is no divergence. Newton-Raphson method describes quadratic equations with asymptotes (Zienkiewicz et al., 2005).

2.4 Loading history

The Exterior Beam-Column Joint models were subjected to constant axial and lateral cyclic loads similar to the condition in the experimental program (Saghafi and Shariatmadar, 2018), as represented in Fig. 12. The constant axial load was $0.15\, f_c' A_g$ and the cyclic lateral loads were based on displacement control according to ACI 374.1-05 (2019) code. According to the previous study (Budiono et al., 2019), in numerical modeling, the hysteretic curves of the first cycle were similar to the second and third ones. Therefore, one cycle per drift ratio could be applied to simplify loading history, as shown in Fig. 13. The modeling results were hysteretic curves that represented a correlation between lateral load and displacement. Wang, et al. (2019) reported that the hysteresis curve reflects changes in strength, stiffness, energy dissipation, and ductility according to the load transfer in each cycle.

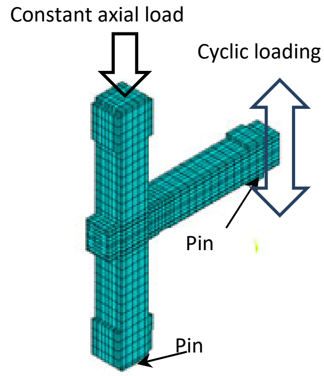

Fig. 12. Loading setup

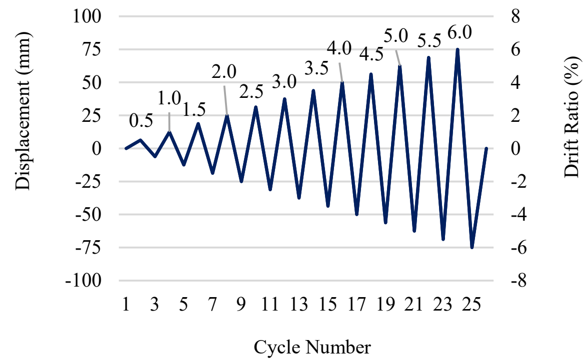

Fig. 13. Loading history

3. Results and discussion

3.1. Modeling Verification

The hysteretic curve of an Exterior Beam-Column Joint (EBJ) modeling using Normal Concrete (NC) was compared with the experimental program of EBJ-NC that had been conducted by previous researchers (Saghafi and Shariatmadar, 2018). The detail of reinforcement of EBJ-NC was described in Fig. 1. The difference between the maximum loads of the model and the experimental specimen did not exceed 10%. Then it satisfied the accuracy (Badshah, et al., 2019). The differences between the maximum lateral load of the numerical model and the experimental program, in the direction of push and loads, were 7.737% and 3.386%, respectively, as written in Table 3.

Table 3. Percentage of different values of the maximum lateral loads

Load Direction	Experiment		Numerical model		Drift Ratio	Difference of max. loads
	Max. lateral load	Displacement	Max. lateral load	Displacement		
	(kN)	(mm)	(kN)	(mm)	(%)	(%)
Push	38.00	31.25	35.06	32.36	2.5	7.737
Pull	-37.57	-43.75	-36.11	-45.37	-3.5	3.886

The stresses of structural members may exceed the yield strength due to cyclic lateral loads. It happens because of high loads that make the structure yield. The stress condition of the EBJ-NC is shown in Figs. 14 and 15. The EBJ-NC model without shear reinforcement in the joint zone could withstand compressive stresses of 14.44 to 0.55 MPa.

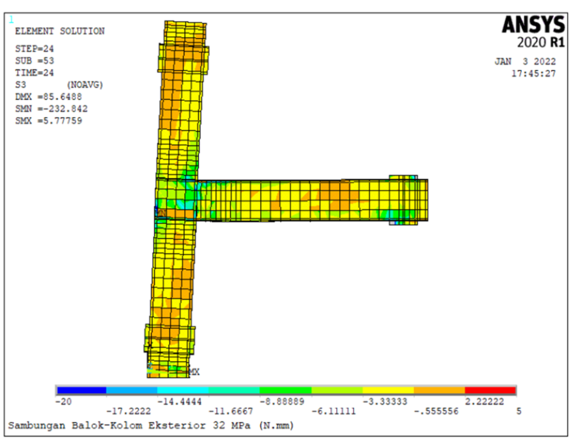

Fig. 14. Stress contour of EBJ-NC model in drift ratio of 6% under push loading

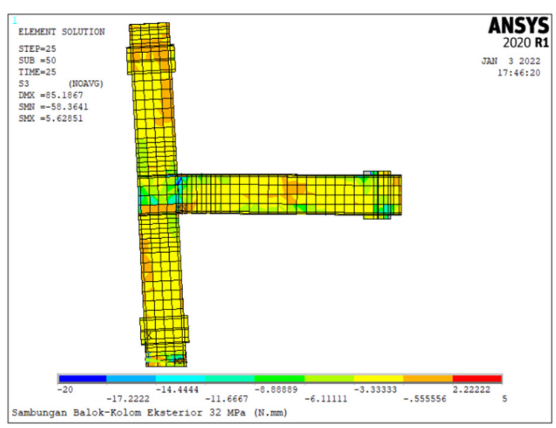

Fig. 15. Stress contour of EBJ-NC model in drift ratio of 6% under pull loading

3.2 Exterior Beam-Column Joints Using Self Compacting Concrete

The hysteresis curves of three EBJ models using SCC material (EBJ-S1, EBJ-S2, and EBJ-S3) with a variation of shear reinforcements are shown in Figs. 16, 17, and 18. Under the push loads, the EBJ-S2 model achieved the highest maximum lateral load. It had horizontal shear reinforcements in the joint as concrete confinement. The lowest maximum lateral load was achieved by the EBJ-S1 models that had no shear reinforcement. The EBJ-S3 model had diagonal shear reinforcement that resists tensile and compressive forces when cyclic lateral loads occurred so that it reached a maximum lateral load higher than the EBJ-S1 model (Demir, et al., 2016; Ding, et al., 2017). A different behavior was shown under pull load. The EBJ-S3 with diagonal shear reinforcement performed the highest lateral load and was followed by the EBJ-S1 and EBJ-S2. Table 4 shows the maximum lateral loads and displacement of all BJC using SCC models. The stability of strength of EBJ-S2 made it achieve the highest drift ratio of 3.5% under the maximum lateral push load. For a comparison, the EBJ-S1 and EBJ-S3 only achieved drift ratios of 2.5% and 3.0%, respectively, when the maximum lateral push load occurred. The different behavior was shown under maximum pull lateral loads where EBJ-S1, EBJ-S2, and EBJ-S3 models achieved the same drift ratio of 3.5%.

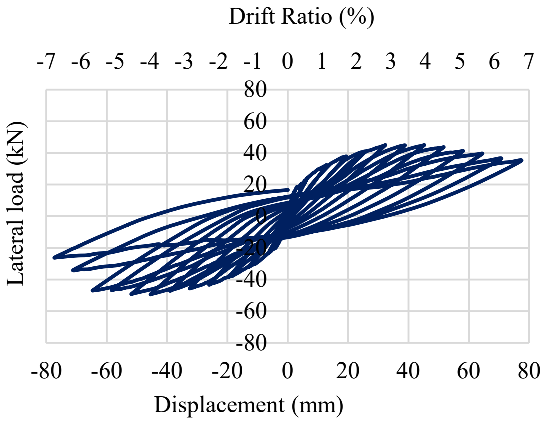

Fig. 16. Hysteretic curves of EBJ-S1

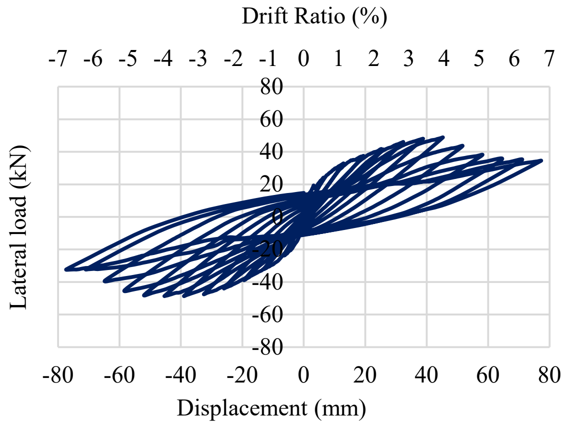

Fig. 17. Hysteretic curves of EBJ-S2

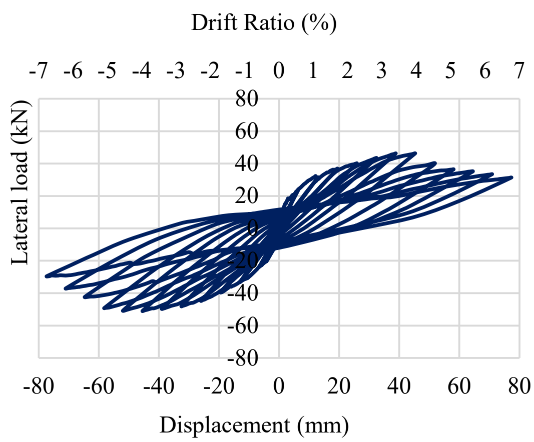

Fig. 18. Hysteretic curves of EBJ-S3

Table 4. The maximum lateral loads of the Exterior Beam-Column Joint numerical models using Self Compacting Concrete (EBJs-SCC)

Model	Load direction	Peak deformation Δ_{max} (mm)	Story drift (%)	Maximum load F_{max} (kN)	Average of maximum loads $\bar{F}_{max}$ (mm)
EBJ-S1	Push	44.920	2.5	32.370	47.121
	Pull	-49.322	3.5	-45.466	
EBJ-S2	Push	48.812	3.5	45.2517	48.747
	Pull	-48.682	3.5	-45.423	
EBJ-S3	Push	46.241	3.0	38.817	48.601
	Pull	-50.961	3.5	-45.463	

3.3 Stress Contours

The EBJ-S1 model with no shear reinforcement in the joint could only withstand compressive stresses ranging from 3.33 to 17.22 MPa, as shown in Fig. 19 and Fig. 20. Fig. 21 and Fig. 22 show that the EBJ-S2 model with horizontal shear reinforcement achieved compressive stresses of 3.33 to 20 MPa.

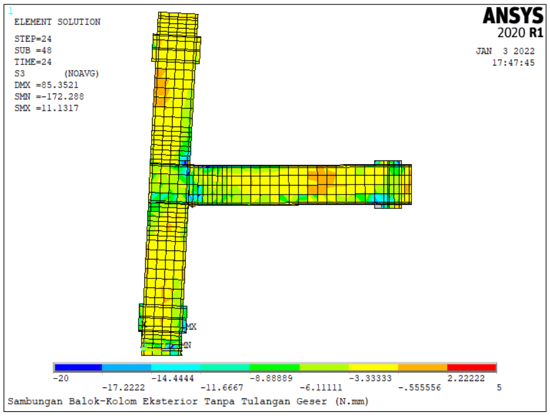

Fig. 19. Stress contour of EBJ-S1 in drift ratio of 6% under push load

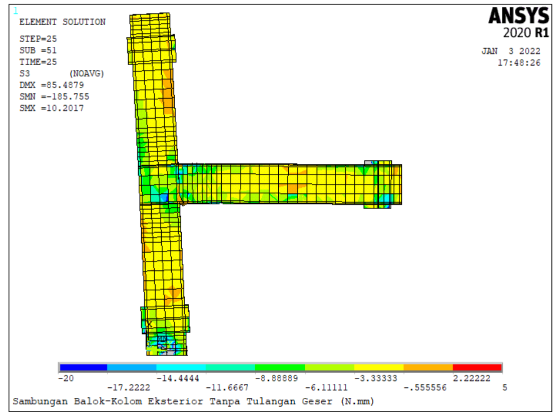

Fig. 20. Stress contour of EBJ-S1 in drift ratio of 6% under pull load

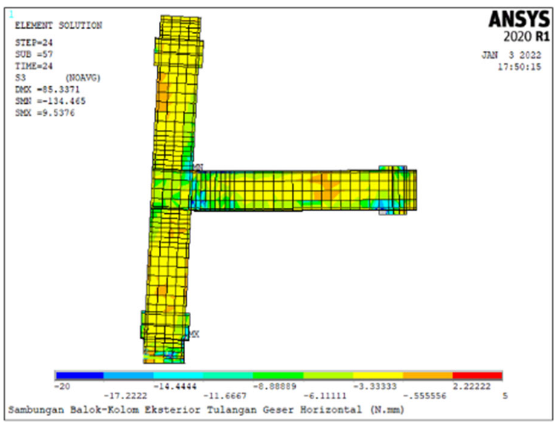

Fig. 21. Stress contour of EBJ-S2 in drift ratio of 6% under push load

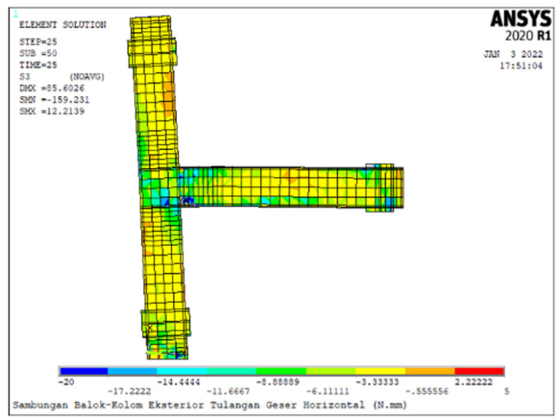

Fig. 22. Stress contour of EBJ-S2 in drift ratio of 6% under pull load

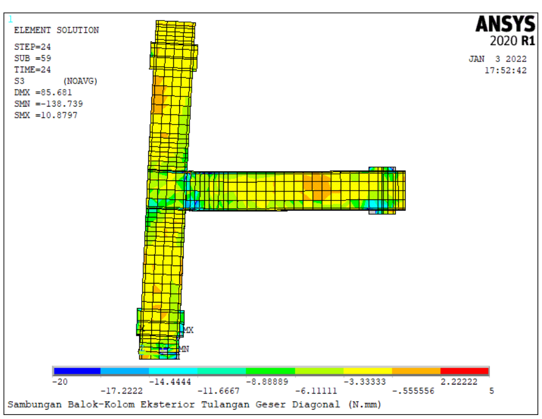

Fig. 23. Stress contour of EBJ-S3 in drift ratio of 6% under push load

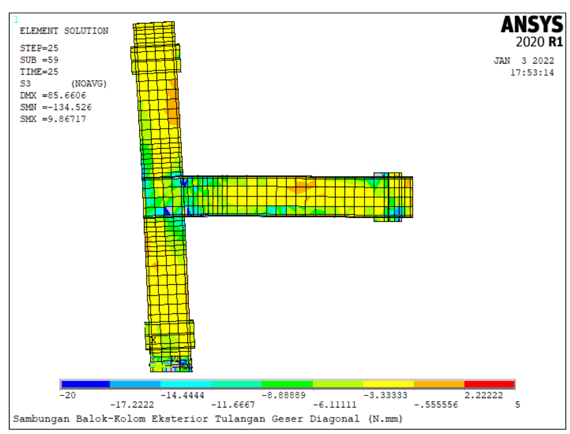

Fig. 24. Stress contour of EBJ-S3 in drift ratio of 6% under pull load

The EBJ-S3 model with diagonal shear reinforcement in the joint could withstand compressive stress of 3.33 to 20 MPa over a wider area of EBJ-S2's. This condition is shown in Figs. 23 and 24. There was no shear reinforcement in the joint of EBJ-S1. Then, the EBJ-S1 model failed to resist stress in the joint due to low capacity to confine concrete. It made the structure unable to confine the concrete. This condition was crushing large quantities of concrete simultaneously when subjected to cyclic lateral loads. The EBJ-S2 model formed plastic hinges on the beam. This mechanism occurred because the horizontal shear reinforcements were designed based on seismic criteria and applied in the joint. It made the structure able to confine the concrete under cyclic lateral loading. Then the structure did not experience joint failure. The stress contour showed that the EBJ-S3 model had more concrete crushing but less diagonal cracking than the EBJ-S2 model. The diagonal shear reinforcement in the joint of the EBJ-S3 model confined the concrete in the diagonal directions but was more fragile in the horizontal direction. In general, the concrete crack patterns of all models were diagonal. It harmonized with the function of the diagonal reinforcement in the joint to minimize the diagonal cracks when the EBJs resisted cyclic lateral loads.

3.4 Displacement Ductility

Ductility is closely related to the ability of a structure to dissipate earthquake energy. A structure with a high ductility value can dissipate earthquake energy better. Thus, the ability of the structure to deform under inelastic conditions is getting better. The higher ultimate deformation under inelastic conditions results in increased ductility and energy dissipation and better structural performance in resisting earthquake loads. The ductility value is determined from the elastic and yield conditions (Choi et al., 2022; Park, 1989; Nurjannah et al., 2022). There are four kinds of ductility, namely the type of strain, curvature, displacement, and rotation (Park & Paulay, 1992). The yield point was determined using FEMA 356 (2000) based on the equal area method. The dividing line between the lateral load and the displacement should equal the area between the upper and lower curves. The yield, peak, and ultimate lateral loads and deformations of the EBJ-NC from the numerical model are shown in Fig. 25. Table 5 shows both ductility values under push and pull lateral loads were included in the high ductility category since they were more than 4. The joint zone of EBJ-NC had no shear reinforcement making the structural elements more flexible under lateral loading and deformed.

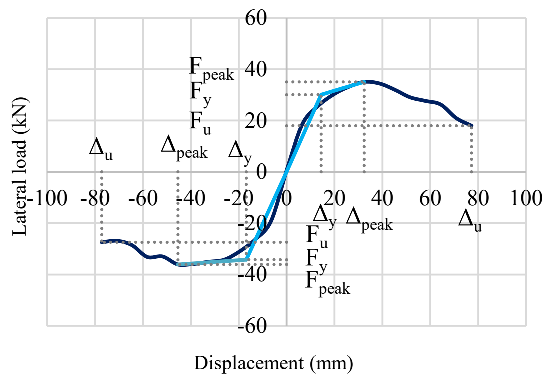

Fig. 25. The envelope curve of the EBJ-NC

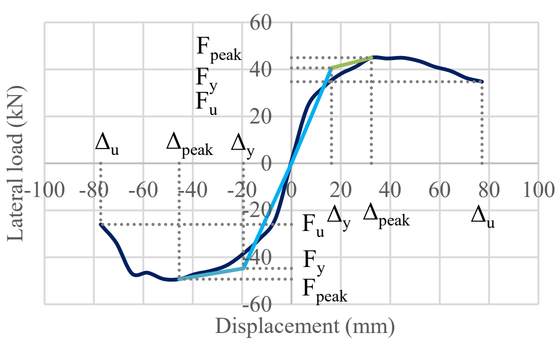

Fig. 26. The envelope curve of EBJ-S1

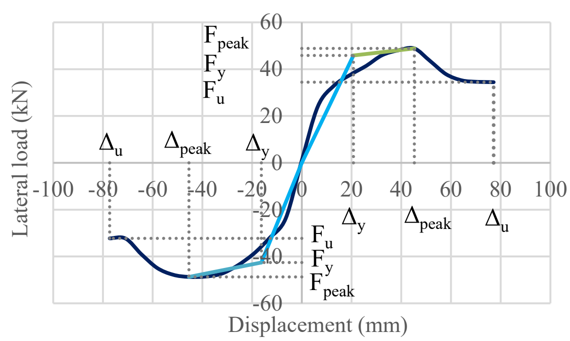

Fig. 27. The envelope curve of EBJ-S2

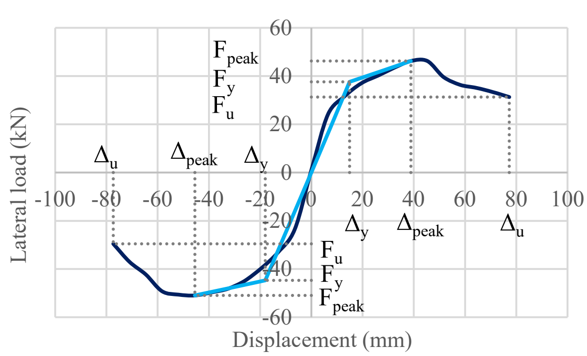

Fig. 28. The envelope curve of EBJ-S3

Tabel 5. Displacement ductility of the Exterior Beam-Column Joint numerical model using Normal Concrete (EBJ-NC)

Load direction	Ultimate deformation	Yield deformation	Ductility	Average ductility
	Δ_u (mm)	Δ_y (mm)	μ	$\bar{\mu}$
Push	77.248	14.385	5.370	4.974
Pull	-77.209	-16.867	4.578	

The method of determining yield points of all EBJ-SCC models was also based on the same code (FEMA 356, 2000). The position of the yield points of EBJ-S1, EBJ-S2, and EBJ-S3 models are presented in Figs. 26, 27, and 28. The variation of shear reinforcement affected the yield deformations and lateral loads, as shown in Table 6. Each peak of push and the pull-lateral load of story drifts are resumed in Table 4.

Tabel 6. Displacement ductility of the Exterior Beam-Column Joint numerical models using Self Compacting Concrete

Model	Load direction	Ultimate deformation	Yield deformation	Ductility	Average ductility
		Δ_u (mm)	Δ_y (mm)	μ	$\bar{\mu}$
EBJ-S1	Push	77.180	16.219	4.758	4.362
	Pull	-77.277	-19.491	3.965	
EBJ-S2	Push	77.174	20.798	3.711	4.232
	Pull	-77.306	-16.262	4.754	
EBJ-S3	Push	77.256	14.955	5.166	4.733
	Pull	-77.317	-17.981	4.300	

The average ductility of EBJ-S3 was greater than the EBJ-S1 and EBJ-S2 models due to the strength of diagonal shear reinforcements in the joint zone. Then the EBJ-S1 model was more flexible than the EBJ-S1 and EBJ-S2 models to achieve higher ultimate displacement. The EBJ-S1 had no shear reinforcement, making it more vulnerable to resisting lateral load through a shear mechanism in the joint zone. This condition caused the EBJ-S1 model to experience yield faster than the other two models. The EBJ-S2 was constrained by the horizontal shear reinforcements that made it reach less ultimate deformation than EBJ-S1 and EBJ-S3. The ductility values of the EBJ-S1 and EBJ-S2 models are not much different. It showed that the EBJ-S1 model still performed ductile behavior without shear reinforcement in the joint. This behavior is similar with the EBJ-NC specimen in the experimental program (Saghafi and Shariatmadar, 2018). However, EBJ-S1 model only reached the lowest peak lateral loads compared with EBJ-S2 and EBJ-S3. The horizontal shear reinforcement of EBJ-S2 provides adequate strength to achieve the highest average lateral peak load. The diagonal shear reinforcement of EBJ-S3 provided a certain strength that made it achieve a relatively closed average lateral load with EBJ-S2. These results also showed that the EBJ-S1 model ductility value was less than the EBJ-NC's. It was due to NC material being more ductile than SCC materials. However, all models of EBJ using SCC materials performed high ductility since all values were more than 4 (FEMA 356, 2000).

3.5 Stiffness Degradation

The stiffness values were obtained from the ratio between lateral loads and displacements (Essa, 2018; Ma, et al., 2021). The strength of the structure is the maximum lateral load at each drift ratio that forms the backbone curve. The correlation between the stiffness value and drift ratio of the EBJ-NC model is shown in Fig. 29. The stiffness decreased due to the inability to withstand the lateral loads. This condition occurred along with the increased drift ratios. Fig. 29 also compares the stiffness degradation of EBJ-NC and EBJ-S1 models with the exact detail of dimension and reinforcement, but different materials of Normal Concrete and Self Compacting Concrete. The EBJ-S1 model performed higher stiffness than EBJ-NC, both under push and pull lateral loads from the initial until the last drift ratios. It was because the higher compressive strength and concrete elastic modulus of Self Compacting Concrete than Normal Concrete provided stiffer and stronger structures (Choi, et al., 2022) from the initial until the ultimate drift ratios.

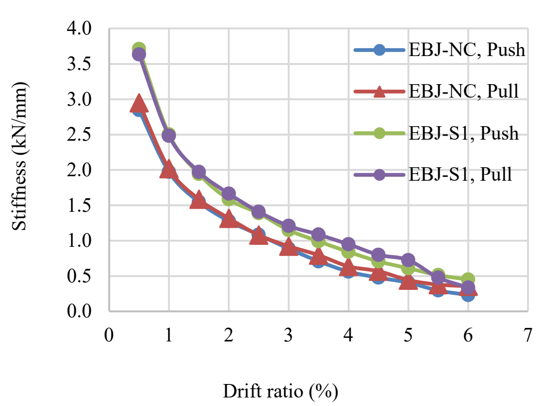

Fig. 29. Stiffness degradation of EBJs using Normal Concrete and Self Compacting Concrete under push and pull loads

Fig. 30 shows the stiffness degradation of all the EBJ-SCC models under push loads. The stiffness values of EBJ-S1, EBJ-S2, and EBJ-S3 models were relatively the same in a drift ratio of 0.5%. Then, the EBJ-S1 and EBJ-S3 experienced faster stiffness degradation since the drift ratio of 1.0%. The EBJ-S2 model showed higher stiffnesses than EBJ-S1 and EBJ-S3 until the ultimate drift ratio of 6.0%. This behavior was because EBJ-S2 had the stronger horizontal shear reinforcement in the joint zone that confined the concrete under cyclic lateral loads. The EBJ-S1 had no shear reinforcement to confine the concrete in the joint zone, while the diagonal shear reinforcement of EBJ-S3 performance was below the EBJ-S2's horizontal shear reinforcement. Fig. 31 shows all the EBJ-SCC models' stiffness values under the pull loads. The crack propagation influenced the concrete elements in resisting pull loads, resulting in a weaker structure under pull loads in the same drift ratios. This behavior continued until the ultimate drift ratio of 6.0%. Table 7 shows the more accurate stiffness values of all EBJ models.

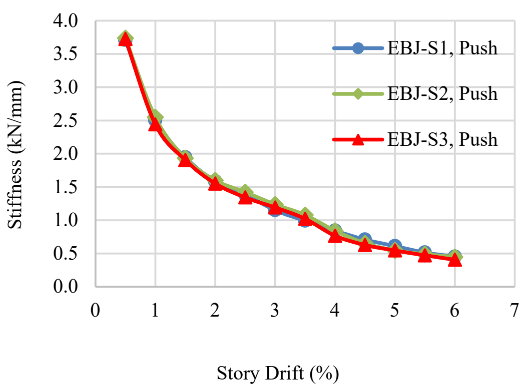

Fig. 30. Stiffness degradation of EBJs using Self Compacting Concrete under push loads

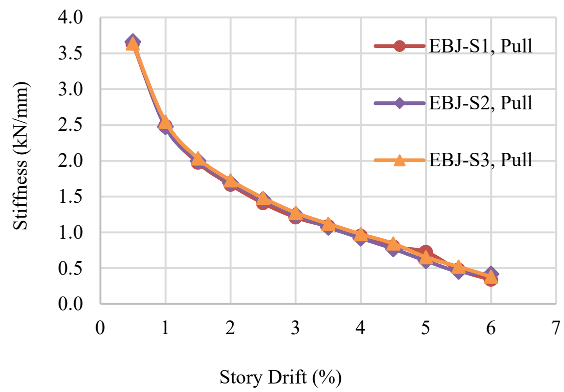

Fig. 31. Stiffness degradation of EBJs using Self Compacting Concrete under pull loads

Table 7. Stiffness of the Exterior Beam-Column Joint using Normal Concrete (EBJ-NC) and Self Compacting Concrete (EBJ-S1, EBJ-S2, and EBJ-S3)

	Stiffness (kN/mm)							
Drift ratio	EBJ-NC	EBJ-NC	EBJ-S1	EBJ-S1	EBJ-S2	EBJ-S2	EBJ-S3	EBJ-S3
(%)	Push	Pull	Push	Pull	Push	Pull	Push	Pull
0.5	2.847	2.949	3.710	3.632	3.738	3.660	3.726	3.634
1.0	1.973	2.018	2.503	2.482	2.547	2.473	2.441	2.546
1.5	1.548	1.585	1.944	1.972	1.933	1.997	1.904	2.033
2.0	1.279	1.317	1.585	1.665	1.599	1.689	1.550	1.726
2.5	1.083	1.078	1.388	1.408	1.421	1.458	1.342	1.481
3.0	0.888	0.922	1.150	1.209	1.237	1.247	1.191	1.275
3.5	0.709	0.796	0.992	1.085	1.079	1.072	1.021	1.121
4.0	0.563	0.636	0.842	0.950	0.841	0.921	0.765	0.975
4.5	0.477	0.569	0.708	0.800	0.652	0.770	0.627	0.845
5.0	0.407	0.442	0.610	0.725	0.546	0.603	0.545	0.654
5.5	0.296	0.379	0.513	0.477	0.488	0.455	0.471	0.521
6.0	0.233	0.355	0.450	0.337	0.446	0.417	0.405	0.382

4. Conclusion

The analysis of the four models of Exterior Beam-Column Joints (EBJ) using Normal Concrete (NC) and Self Compacting Concrete (SCC) materials resulted in the following conclusions:

1. The Exterior Beam-Column Joint numerical models using NC and SCC performed high ductility in resisting cyclic lateral loads. All the models achieved the ultimate drift ratio of 6.0%.
2. The EBJ-NC showed the highest ductility of all EBJ-SCC models. It indicated that the NC material was more ductile than SCC.
3. The EBJ-S1 and EBJ-S2 followed the highest ductility of EBJ-S3 due to the strength of diagonal shear reinforcements in the beam-column joint zone. The EBJ-S1 had no shear reinforcement, making it more vulnerable to resist lateral load and causing it to experience yield faster than the other two models. The EBJ-S2 was constrained by the horizontal shear reinforcements that made it reach less ultimate deformation than EBJ-S1 and EBJ-S3.
4. All EBJ-SCC models showed better performance than EBJ-NC model in strength and stiffness under lateral cyclic loads. It was due to the higher concrete compressive strength and elastic modulus of the SCC than NC's.

5. The EBJ-S2 and EBJ-S3 models performed better performance than the EBJ-S1 model. It was because of horizontal and diagonal shear reinforcements in the joint zones of EBJ-S2 and EBJ-S3, respectively, which could prevent joint failure when the EBJs were subjected to cyclic lateral loads.
6. The stress contour showed that the EBJ-S1 only resisted compressive stress of 3.33 to 17.22 MPa due to the absence of shear reinforcement in the joint zone. The EBJ-S2 was able to withstand compressive stress of 3.33 to 20 MPa with the horizontal shear reinforcements. The EBJ-S3 with diagonal reinforcement could resist the same compressive stress of EBJ-S2 in a wider area. However, the concrete crushing occurred more in the EBJ-S3. It indicated that the horizontal and diagonal shear reinforcement in the joint zones of EBJ-S2 and S3, respectively, confined the concrete. Despite the capability of diagonal shear reinforcement to minimize the diagonal crack in the joint, the horizontal shear reinforcement provided better performance in confining concrete and avoiding concrete crushing.

Acknowledgment

All authors thank Sriwijaya University for the opportunity given to conduct this research.

References

ANSYS, Inc. (2013). ANSYS Mechanical APDL Structural Analysis Guide, Release 15.0.

American Concrete Institute Committee 374. (2019). (reapproved). ACI 374.1-05. Acceptance Criteria for Moment Frames Based on Structural Testing and Commentary, American Concrete Institute, Farmington Hills, MI.

Badshah, M., Badshah, S., & Jan, S. (2020). Comparison of computational fluid dynamics and fluid structure interaction models for the performance prediction of tidal current turbines. *Journal of Ocean Engineering and Science*, *5*(2), 164-172. https://doi.org/10.1016/j.joes.2019.10.001

Budiono, B., Nurjannah, S. A., & Imran, I. (2019). Nonlinear Numerical Modeling of Partially Pre-stressed Beam-column Sub-assemblages Made of Reactive Powder Concrete. *Journal of Engineering and Technological Sciences*, *51*(1), 28-47. https://doi.org/10.5614/j.eng.technol.sci.2019.51.1.3

Brouwers, H. J. H., & Radix, H. J. (2005). Self-compacting concrete: theoretical and experimental study. *Cement and concrete research*, *35*(11), 2116-2136. https://doi.org/10.1016/j.cemconres.2005.06.002

Choi, S. H., Kim, J. H., Jeong, H., & Kim, K. S. (2022). Seismic behavior of beam-column joints with different concrete compressive strengths. *Journal of Building Engineering*, *52*, 104484. https://doi.org/10.1016/j.jobe.2022.104484

Concrete, S. C. (2005). The European guidelines for self-compacting concrete. *BIBM, et al*, *22*, 563.

Cook, R. D. (2007). *Concepts and applications of finite element analysis*. John wiley & sons.

Demir, A., Caglar, N., Ozturk, H., & Sumer, Y. (2016). Nonlinear finite element study on the improvement of shear capacity in reinforced concrete T-Section beams by an alternative diagonal shear reinforcement. *Engineering Structures*, *120*, 158-165. https://doi.org/10.1016/j.engstruct.2016.04.029

Ding, R., Tao, M. X., Nie, X., & Mo, Y. L. (2017). Fiber beam-column model for diagonally reinforced concrete coupling beams incorporating shear and reinforcement slip effects. *Engineering Structures*, *153*, 191-204. https://doi.org/10.1016/j.engstruct.2017.10.035

Essa, S. (2018). Analysis of elastic beams on linear and nonlinear foundations using finite difference method. *Eurasian Journal of Science and Engineering*, *3*(3), 92-101.

FEMA 356, F. E. (2000). Prestandard and commentary for the seismic rehabilitation of buildings. *FEMA Publication No*, *356*.

Ghouilem, K., Mehaddene, R., Ghouilem, J., Kadri, M., & Boulifa, D. (2022). ANSYS modeling interface and creep behavior of concrete matrix on waste glass powder under constant static stress. *Materials Today: Proceedings*, *49*, 1084-1092. https://doi.org/10.1016/j.matpr.2021.09.387

Hanafiah, Saloma, & Whardani, P. N. K. (2017, November). The behavior of self-compacting concrete (SCC) with bagasse ash. In *AIP Conference Proceedings* (Vol. 1903, No. 1, p. 050005). AIP Publishing LLC. https://doi.org/10.1063/1.5011544

Islam, G. S., Akter, S., & Reza, T. B. (2022). Sustainable high-performance, self-compacting concrete using ladle slag. *Cleaner Engineering and Technology*, *7*, 100439. https://doi.org/10.1016/j.clet.2022.100439

Jagota, V., Sethi, A. P. S., & Kumar, K. (2013). Finite element method: an overview. *Walailak Journal of Science and Technology (WJST)*, *10*(1), 1-8.

Jayaseelan, R., Pandulu, G., & Mahendran, S. (2021). Performance of expanded polystyrene light weight self compacting concrete in composite slab. *International Journal of Applied Science and Engineering*, *18*(1), 1-12. https://doi.org/10.6703/IJASE.202103_18(1).007

Karthik, J., Surendra, H. J., Anusha, M., & Prathibha, V. S. (2022). Assessment of self-compacting concrete without super plasticizer in bridge construction. *Materials Today: Proceedings*. https://doi.org/10.1016/j.matpr.2022.04.516

Ma, T., Zhang, L., & Xu, L. (2021). Effects of beam axial deformations on storey-based critical gravity loads in tension-only semi-braced steel frames. *Engineering Structures*, *232*, 111862. https://doi.org/10.1016/j.engstruct.2021.111862

Nurjannah, S. A., Putri, N. D., & Albimanzura, F. S. (2022). Numerical analysis of lightweight concrete wall panels having a variation of dimensions and openings that were subjected to static lateral loads. *Journal of Applied Engineering Science*, *20*(1), 109-122. https://doi.org/10.5937/jaes0-31011

Park, R. (1989). Evaluation of ductility of structures and structural assemblages from laboratory testing. *Bulletin of the new Zealand society for earthquake engineering*, *22*(3), 155-166. https://doi.org/10.5459/bnzsee.22.3.155-166

Paulay, T., & Priestley, M. N. (1992). Seismic design of reinforced concrete and masonry buildings. John wiley & sons.

Pinto, V., Rocha, L., Santos, E., & Isoldi, L. (2022). Numerical analysis of stiffened plates subjected to transverse uniform load through the constructal design method. *Engineering Solid Mechanics*, *10*(1), 99-108. DOI: 10.5267/j.esm.2021.9.001

Hossein Saghafi, M., & Shariatmadar, H. (2018). Enhancement of seismic performance of beam-column joint connections using high performance fiber reinforced cementitious composites. *Construction and Building Materials*, *180*, 665-680. https://doi.org/10.1016/j.conbuildmat.2018.05.221

Standard, A. A. (2011, August). Building Code Requirements for Structural Concrete (ACI 318-11). In *American Concrete Institute*.

Thompson, M. K., & Thompson, J. M. (2017). *ANSYS mechanical APDL for finite element analysis*. Butterworth-Heinemann.

Verzegnassi, E., Altheman, D., Gachet, L. A., & Lintz, R. C. C. (2022). Study of the properties in the fresh and hardened state of self-compacting lightweight concrete. *Materials Today: Proceedings*. https://doi.org/10.1016/j.matpr.2022.04.403

Wang, B., Huo, G., Sun, Y., & Zheng, S. (2019). Hysteretic behavior of steel reinforced concrete columns based on damage analysis. *Applied Sciences*, *9*(4), 687.

Zienkiewicz, O. C., Taylor, R. L., & Zhu, J. Z. (2005). *The finite element method: its basis and fundamentals*. Elsevier.